Strong Exciton-Photon Coupling and Exciton Hybridization in a Thermally Evaporated Polycrystalline Film of an Organic Small Molecule

R. J. Holmes and S. R. Forrest

Princeton Institute for the Science and Technology of Materials (PRISM), Department of Electrical Engineering,
Princeton University, Princeton, New Jersey 08544, USA
(Received 1 April 2004; published 28 October 2004)

We demonstrate strong exciton-photon coupling in an optical microcavity containing a thermally evaporated polycrystalline organic thin film. Microcavity polaritons result from coupling between the 0-0 excitonic transition of 3,4,7,8 napthalenetetracarboxylic dianhydride and a cavity photon. For thicker films, the 0-1 transition also couples to the cavity mode, as vibronic relaxation is overcome by the short Rabi period for strong coupling. To our knowledge, this is the first report of strong coupling between a cavity photon and multiple vibronic transitions in a single material, made possible by the pronounced vibronic absorption features characteristic of crystalline organic materials.

Since the first demonstration of strong exciton-photon coupling in an optical microcavity (OMC) [1], there has been significant interest in the study of microcavity polaritons. In this work, OMCs containing the thermally evaporated polycrystalline organic 3,4,7,8 napthalenetetracarboxylic dianhydride (NTCDA) [2] exhibit strong coupling and the hybridization of excitons arising from separate vibronic transitions characteristic of this molecular species. Indeed, organic films deposited by thermal evaporation offer a unique means for exploring the strongly coupled state: namely, the ability to examine polaritonic processes as a function of film morphology and hence phonon coupling strength in a single material.

For strong coupling to be observed, narrow absorption features are required, implying long exciton lifetimes during which coupling to the cavity photon can occur. Hence, observation of strong coupling in thermally evaporated polycrystalline thin films was thought to be difficult or even impossible due to their characteristically broad and featureless transition linewidths that arise from strong intermolecular interactions [2]. For this reason, the study of microcavity polaritons in organic semiconductors has, until now, been confined to materials that have been spun cast to form a thin film [3–7]. Doping organic materials at low concentrations into a polymer matrix decreases the interaction between guest molecules, often resulting in a reduction of the transition linewidth. To our knowledge, this is the first report of strong coupling in a thermally evaporated, crystalline organic thin film, and of coupling between separate, multiple vibronic transitions in a single material, made possible by their narrow and intense spectral lines. This work opens up new avenues for the understanding and application of strongly coupled states in this important class of semiconductor materials.

To observe large optical gain in strongly coupled media [8,9], we require efficient scattering from large wave vector to zero wave vector states. This process is often inhibited by the polariton relaxation bottleneck [10]. In organic materials, an additional relaxation pathway to the zero wave vector state is available: namely, phonon assisted relaxation. The use of a thermally evaporated organic film allows for a range of active medium morphologies, from amorphous to polycrystalline, and, consequently, allows for a range of phonon coupling strengths. Hence, crystalline or polycrystalline active media may enhance the strength of the phonon assisted relaxation in the lower polariton branch, thus allowing for a more efficient population of the zero wave vector state.

Distributed Bragg reflectors (DBR) consisting of eight pairs of quarter wavelength thick SiO_2 and SiN_x layers were deposited on quartz substrates using plasma enhanced chemical vapor deposition, yielding a peak reflectivity of 95%. A polycrystalline film [11] of NTCDA was deposited onto the DBR mirror by sublimation at 10^{-7} Torr, forming a cavity between the DBR and a 200 nm Al cap deposited onto the NTCDA surface by thermal evaporation. The closely spaced and pronounced 0-0 and 0-1 absorptive vibronic transitions of NTCDA allow them both to be accessed within a single DBR cavity mode. The dispersion relation of each OMC was determined by using angularly resolved reflection spectroscopy, measuring sample reflectivity as a function of excitation wavelength and angle [12]. Angular reflectivity spectra were collected under illumination through the quartz substrate with *p*-polarized, monochromated white light using a spectroscopic ellipsometer at room temperature.

The inset of Fig. 1 depicts the room temperature absorbance and photoluminescence emission spectrum of an NTCDA film. The full-width at half-maximum linewidths of the 0-0 (3.19 ± 0.05 eV) and 0-1 (3.39 ± 0.05 eV) transitions are (145 ± 5) meV and $(138 \pm$

5) meV, respectively, while the Stokes shift between the 0-0 absorption and emission lines is approximately 30 meV. The 0-0 and 0-1 transitions arise from absorption from the S_0 ground state vibronic level to either the lowest or the first vibronic level of the S_1 excited state.

Reflectivity spectra from an OMC containing a 20 nm thick film of NTCDA exhibit two clearly defined features, with anticrossing at an angle of $\theta = 28°$ (Fig. 1). Reflectivity peak energies were extracted using Gaussian fits to the multiple absorption features. Both branches of the peak dispersion in Fig. 1 were fit by a conventional two-level interaction Hamiltonian [13], yielding the energy eigenvalues:

$$\varepsilon = \frac{(E_p + E_{ex})}{2} \pm \frac{1}{2}\sqrt{(E_p - E_{ex})^2 + 4V^2}. \qquad (1)$$

The potential, V, includes the interaction of the exciton and the cavity photon. Here the uncoupled exciton dispersion (E_{ex}) is independent of angle, with the cavity photon energy, E_p, following [14]:

$$E_p = E_0\left(1 - \frac{\sin^2\theta}{n^2}\right)^{-1/2}, \qquad (2)$$

where the cutoff energy is E_0, and n is the effective index of refraction of the uncoupled and nonabsorbing cavity. The fits in Fig. 1 were obtained following Eqs. (1) and (2) using the parameters listed in Table I, yielding $V = (78 \pm 2)$ meV. Since V is related to the normal mode Rabi splitting (i.e., $V = \Omega/2$ [13], then $\Omega = (156 \pm 4)$ meV.
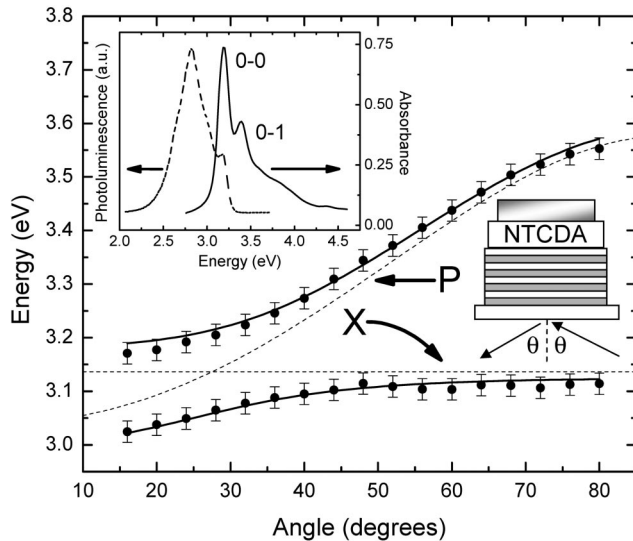
FIG. 1. Dispersion relation for an organic microcavity with a 20 nm thick NTCDA active layer. The broken curves are the uncoupled photon (P) and exciton (X) dispersion relations as determined by the fitting parameters of Table I and Eq. (2). Inset: Room temperature photoluminescence and absorbance spectra for a 50 nm thick film of NTCDA. Absorption peaks at 3.19 and 3.39 eV are designated as the 0-0 and 0-1 transitions.

Microcavities with 40 and 60 nm thick active layers were also fabricated. In general, Ω varies as $(\alpha L)^{1/2}$, where α and L are the absorption coefficient and thickness of the NTCDA layer, respectively [1]. Reflectivity spectra collected at selected angles for these microcavities are depicted in Fig. 2. Aside from the features arising from coupling between the cavity mode and the 0-0 transition of NTCDA, a third feature is also observed at higher energy, consistent with coupling to the 0-1 transition of NTCDA, yielding the dispersion relations in Fig. 3. Anticrossing between branches is observed, and both the middle and the upper branches asymptotically approach their respective uncoupled exciton energies at low angle. The middle branch of the dispersion relation for both thicknesses becomes clearly visible at $\theta > 20°$, whereas the top branch is observed at $\theta > 35°$, where this branch acquires significant photon character (Fig. 4).

The coupled mode formalism can be extended to include a third excitonic oscillator via [15–17]

$$\begin{bmatrix} E_p & V_1 & V_2 \\ V_1 & E_{ex1} & 0 \\ V_2 & 0 & E_{ex2} \end{bmatrix} \begin{bmatrix} \alpha \\ \beta \\ \gamma \end{bmatrix} = \varepsilon \begin{bmatrix} \alpha \\ \beta \\ \gamma \end{bmatrix}, \qquad (3)$$

where α, β, and γ are the mixing coefficients of the new eigenvectors of the strongly coupled system. Here, two interaction potentials (V_1, V_2) are included in the Hamiltonian as well as two separate uncoupled exciton energy states (E_{ex1}, E_{ex2}). The energy eigenvalues can be determined numerically to model the dispersion relations of Fig. 3 (solid lines), yielding the parameters in Table I. Here, E_{ex1} is fixed to the value obtained from the 20 nm film, and E_{ex2} is held constant for both the 40 and 60 nm films. Branch splittings of $\Omega_{0-0} = (280 \pm 20)$ meV and $\Omega_{0-1} = (100 \pm 20)$ meV for the 40 nm film and $\Omega_{0-0} = (360 \pm 20)$ meV and $\Omega_{0-1} = (120 \pm 20)$ meV for the 60 nm film scale with thickness following $(60 \text{ nm}/40 \text{ nm})^{1/2} = 1.22$, as expected.

In Fig. 4, the mixing coefficients $|\alpha|^2$, $|\beta|^2$, and $|\gamma|^2$ [from Eq. (3)] are plotted versus angle for each branch of the dispersion relation for the 40 nm thick film. The lower branch (Fig. 4, top) has symmetrically varying amounts of cavity photon and Ex_1 (0-0 transition) character, with no Ex_2 (0-1 transition) mixing. At the point of strongest

TABLE I. Model parameters for 20, 40, and 60 nm films.[a]

Thickness (nm)	E_0 (eV)	n	V_1 (meV)[b]	V_2 (meV)
20	3.04 ± 0.05	1.90 ± 0.05	78 ± 2	
40	2.88 ± 0.05	1.80 ± 0.05	140 ± 10	50 ± 10
60	2.70 ± 0.05	1.60 ± 0.05	180 ± 10	60 ± 10

[a]Best fits were obtained with uncoupled exciton energies fixed at $E_{ex1} = 3.14$ eV and $E_{ex2} = 3.35$ eV for all thicknesses.
[b]Rabi splittings are equal to twice the interaction potentials V_1 and V_2.
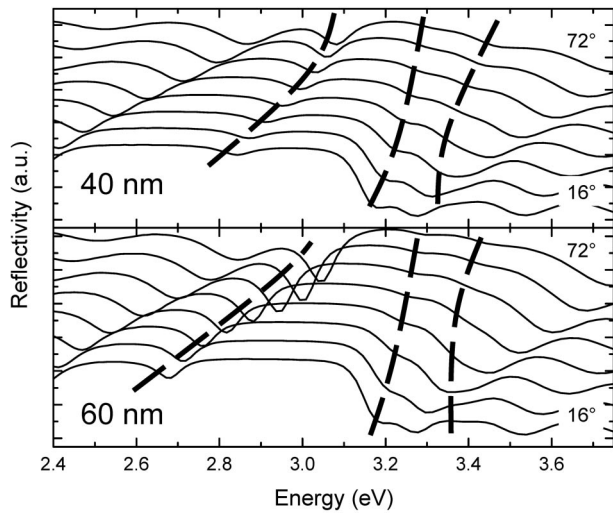
FIG. 2. Reflectivity spectra versus angle of incidence, θ, for devices consisting of 40 nm (top) and 60 nm (bottom) thick NTCDA films. Broken lines indicate a third, high energy feature in the dispersion relation consistent with strong coupling to the 0-1 transition of NTCDA.

coupling ($\theta \sim 50°$), there is significant mixing between the cavity photon and both excitons for the middle branch. Equal coupling is never achieved, although sufficient mixing is present to identify the excitonic states as hybridized. Finally, mixing is observed between the cavity photon and Ex_2 in the upper branch (bottom, Fig. 4). As the branches extend to large angles, some mixing of the Ex_1 state also becomes apparent, likely a result of the strong coupling between the cavity and Ex_1.
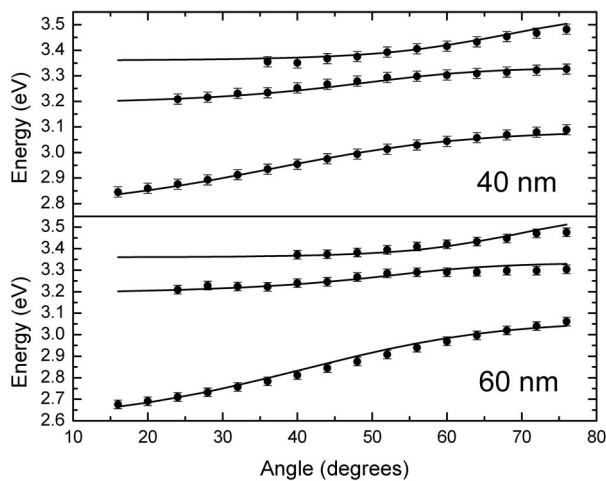
Strong coupling in a polycrystalline organic material such as NTCDA tests the conventional application of the coupled mode formalism of Eq. (3). In NTCDA, since the cavity photon and exciton modes cannot be separated, it is impossible to define an "empty-cavity" regime between the mirrors. The index of refraction, n, used in Eq. (2) is that found in the absence of the absorber, a decoupled scheme that is not experimentally realizable in NTCDA. Hence, since the excitation is near the dispersion edge of NTCDA, the best fits to the data require that n be decreased slightly with increased film thickness as a result of the lower cavity photon energies intrinsic to thicker cavities.

Equation (3) assumes that no coupling between the 0-0 and 0-1 excitonic states exists in the absence of the cavity mode. The large splittings between the middle and upper branches (~ 100 meV) reinforce this notion since coupling would not be observed due to competition with energy transfer between the excitonic states. Observation of exciton hybridization between neighboring vibronic transitions offers a new means to study the rate of vibronic relaxation in organic materials. For 40 and 60 nm thick films, the rate of strong coupling dominates the rate of vibronic relaxation from the first excited vibronic state, for 20 nm thick films, coupling to the 0-1 transition is overcome by vibronic relaxation to the ground vibronic state. The Rabi period for a 40 nm thick film gives a lower limit estimate of the lifetime of the first excited vibronic state. More accurate estimates can be made by measuring the Rabi period as a function of film thickness or concentration in a transparent host (and hence coupling strength); the Rabi period prior to strong coupling being overcome by vibronic relaxation provides an estimate of

FIG. 3. Dispersion relations extracted from the reflectivity spectra in Fig. 2 for 40 and 60 nm thick films. The coupled oscillator model yields splittings of $\Omega_{0-0} = (280 \pm 20)$ meV and $\Omega_{0-1} = (100 \pm 20)$ meV for the 40 nm thick film and of $\Omega_{0-0} = (360 \pm 20)$ meV and $\Omega_{0-1} = (120 \pm 20)$ meV for the 60 nm thick film.
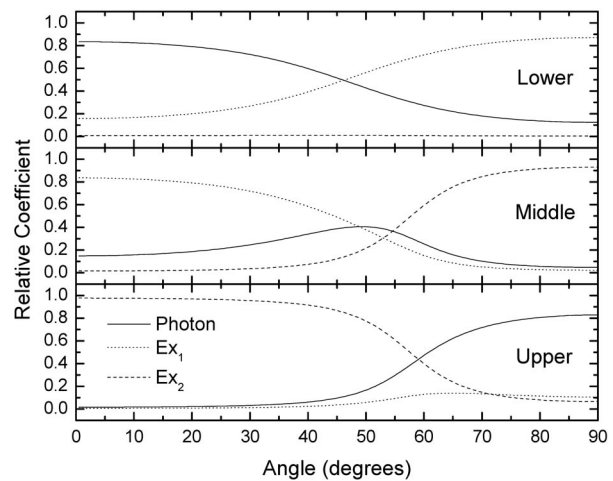
FIG. 4. Mixing coefficients $|\alpha|^2$, $|\beta|^2$, and $|\gamma|^2$ extracted from fits to the 40 nm thick film of Fig. 3. The middle branch has significant mixing between both excitons and the cavity photon at $\theta \sim 50°$. The lower and upper branches of the dispersion relation show contributions from the cavity photon and Ex_1 for the lower branch and Ex_2 for the upper branch.

the lifetime of the first excited vibronic state. This technique should also permit the estimation of the rate of intersystem crossing (ISC) from the singlet to triplet excitonic manifolds for phosphorescent organic molecules, by gradually reducing the strength of coupling to the singlet until the coupling is overcome by ISC to the triplet state.

In strongly coupled organic microcavities, only a fraction of the photogenerated states are thought to be coherent [18]. For example, in J aggregates, it has been suggested that there exists a cutoff wave vector for the lower (upper) branch of the dispersion relation above (below) which states are localized and incoherent [18]. These incoherent states are the result of the broad dispersionless character of electronic transitions in organic semiconductors within an OMC. The incoherent state can be excited nonresonantly, and then radiatively transfer energy to resonantly pump coherent states of the lower branch. This avoids the polariton bottleneck that exists in inorganic materials where exciton-phonon coupling is much weaker, and the uncoupled exciton state is itself coherent. In NTCDA, the exciton linewidth (Fig. 1) is large compared with the Rabi splitting, and hence the majority of the excited states at room temperature are incoherent.

We have demonstrated strong exciton-photon coupling in organic microcavities consisting of a neat, thermally evaporated, polycrystalline small molecule active layer of NTCDA. Large Rabi splittings are observed, and exciton hybridization between a single cavity mode and two neighboring vibronic transitions of NTCDA is understood using a three-body coupled oscillator framework. In addition to exhibiting large Rabi splittings, thermally evaporated polycrystalline films provide a means for understanding effects of morphology and long range order on the strongly coupled state. The observation of strong coupling in polycrystalline materials may allow for increased phonon assisted relaxation to the zero wave vector state as a result of enhanced phonon coupling in the film. This potential for efficient population of the zero wave vector state without the need for stimulated scattering can serve to elucidate the fundamental differences between the strongly coupled state in organic and inorganic semiconductors.

[1] C. Weisbuch, M. Nishioka, A. Ishikawa, and Y. Arakawa, Phys. Rev. Lett. **69**, 3314 (1992).
[2] S. R. Forrest, Chem. Rev. **97**, 1793 (1997).
[3] T. Fujita, Y. Sato, T. Kuitani, and T. Ishihara, Phys. Rev. B **57**, 12 428 (1998).
[4] D. G. Lidzey, D. D. C. Bradley, M. S. Skolnick, T. Virgili, S. Walker, and D. M. Whittaker, Nature (London) **395**, 53 (1998).
[5] D. G. Lidzey, D. D. C. Bradley, T. Virgili, A. Armitage, M. S. Skolnick, and S. Walker, Phys. Rev. Lett. **82**, 3316 (1999).
[6] P. Schouwink, H. V. Berlepsch, L. Dahne, and R. F. Mahrt, Chem. Phys. Lett. **344**, 352 (2001).
[7] N. Takada, T. Kamata, and D. D. C. Bradley, Appl. Phys. Lett. **82**, 1812 (2003).
[8] M. Saba, C. Ciuti, J. Bloch, V. Thierry-Mieg, R. Andre, L. S. Dang, S. Kundermann, A. Mura, G. Bongiovanni, J. L. Staehli, and B. Deveaud, Nature (London) **414**, 731 (2001).
[9] P. G. Savvidis, J. J. Baumberg, R. M. Stevenson, M. S. Skolnick, D. M. Whittaker, and J. S. Roberts, Phys. Rev. Lett. **84**, 1547 (2000).
[10] A. I. Tartakovskii, M. Emam-Ismail, R. M. Stevenson, M. S. Skolnick, V. N. Astratov, D. M. Whittaker, J. J. Baumberg, and J. S. Roberts, Phys. Rev. B **62**, R2283 (2000).
[11] S. R. Forrest, M. L. Kaplan, and P. H. Schmidt, J. Appl. Phys. **56**, 543 (1984).
[12] R. Houdre, C. Weisbuch, R. P. Stanley, U. Oesterle, P. Pellandini, and M. Ilegems, Phys. Rev. Lett. **73**, 2043 (1994).
[13] M. S. Skolnick, T. A. Fisher, and D. M. Whittaker, Semicond. Sci. Technol. **13**, 645 (1998).
[14] A. Yariv, *Optical Electronics in Modern Communications* (Oxford University Press, New York, 1997), 5th ed.
[15] J. Wainstain, C. Delalande, G. Gendt, M. Voos, J. Bloch, V. Thierry-Mieg, and V. Planel, Phys. Rev. B **58**, 7269 (1998).
[16] D. G. Lidzey, D. D. C. Bradley, A. Armitage, S. Walker, and M. S. Skolnick, Science **288**, 1620 (2000).
[17] A. Armitage, M. S. Skolnick, A. Kavokin, D. M. Whittaker, V. N. Astratov, G. A. Gehring, and J. S. Roberts, Phys. Rev. B **58**, 15 367 (1998).
[18] V. M. Agranovich, M. Litinskaia, and D. G. Lidzey, Phys. Rev. B **67**, 085311 (2003).